Wind and Structures, Vol. 12, No. 4 (2009) 299-312
DOI: http://dx.doi.org/10.12989/was.2009.12.4.299

Wind flow around rectangular obstacles with aspect ratio

Hee-Chang Lim*

School of Mechanical, Engineering, PuKyong Nat'l Univ.,
San 100, Yongdang-Dong, Nam-Gu, Busan, 790-784, South Korea

(Received November 3, 2008, Accepted April 3, 2009)

Abstract. It has long been studied about the flow around bluff bodies, but the effect of aspect ratio on the sharp-edged bodies in thick turbulent boundary layers is still argued. The author investigates the flow characteristics around a series of rectangular bodies ($40^d \times 80^w \times 80^h$, $80^d \times 80^w \times 80^h$ and $160^d \times 80^w \times 80^h$ in *mm*) placed in a deep turbulent boundary layer. The study is aiming to identify the extant Reynolds number independence of the rectangular bodies and furthermore understand the surface pressure distribution around the bodies such as the suction pressure in the leading edge, when the shape of bodies is changed, responsible for producing extreme suction pressures around the bluff bodies. The experiments are carried out at three different Reynolds numbers, based on the velocity U at the body height h, of 24,000, 46,000 and 67,000, and large enough that the mean boundary layer flow is effectively Reynolds number independent. The experiment includes wind tunnel work with the velocity and surface pressure measurements. The results show that the generation of the deep turbulent boundary layer in the wind tunnel and the surface pressure around the bodies were all independent of Reynolds number and the longitudinal length, but highly dependent of the transverse width.

Keywords: bluff body; rectangular obstacle; wind environment; surface pressure measurement.

1. Introduction

The flow characteristics on a bluff body immersed in a turbulent flow has long been of fundamental interest in the study of fluid dynamics. Such investigations are critical in the design and development of practical objects such as windmills, buildings and bridges, etc. Over the last several decades this kind of high Reynolds number flow has been considered as a typical design parameter among the construction companies. Above all, the study of flow characteristics around a bluff body is generally considered to be important in academic circles as well as in the engineering applications and now there are still lots of topics left to be studied.

Regarding to the flow around buildings or all kinds, there have been numerous empirical data and comparisons between wind-tunnel and full-scale (field) data. One of the well-cited papers in this area is the wind-tunnel experiments of Castro and Robins (1977) (hereafter denoted by CR), which measured the flow around the surface-mounted cubes. It was one of the first to demonstrate the

* Corresponding Author, E-mail: hclim@pknu.ac.kr

crucial importance of modelling appropriately the details of the upstream boundary layer - *Re* effects existed for smooth upstream flow conditions(i.e. the thickness of the approaching boundary layer was very much smaller than the cube height), whereas for the flow under fully developed turbulent boundary layer, no Re effects were found for $Re > 4000$. That early work was to focus on the importance of ensuring appropriate simulation of the atmospheric boundary layer. There has since been much argument on the Re independency(see e.g. Cherry, *et al*. 1984 and Djilali and Gartshore 1991; more recently Davenport 1999 and Hoxey, *et al*. 1998).

There are some papers to observe the turbulent flow and rectangular bodies interaction. Tieleman and Atkins (1996) reported that the variation of the base/side surface pressure of surface-mounted rectangular prisms was determined by the interaction of the incident turbulence with the separated shear layers, in other words, the small-scale turbulence which could be quantified by the modified parameter, S. This is particularly true for those flows in which the shear layers arising from separation of the boundary layers at the salient edges of the body roll up rapidly to form concentrated relatively steady vortical regions.

More recently, Cigada, *et al*. (2006) investigated the fluid-dynamic forces acting on a rectangular cylinder for unbounded flow conditions. Especially, they focused on the effects of a fixed wall placed at various distances from a rectangular cylinder and observed that the force component acting on the cylinder depends on the periodical motion and provides the dynamic characterization of the loading and of the wake shedding. In addition, the aspect ratio of the body governs effects of the wall condition on the force coefficients and the Strouhal number. Larose and D'Auteuil (2008) made a wind tunnel measurement on rectangular prisms with aspect ratio of 2, 3 and 4 at high Reynolds number, and reported that the Reynolds number effects in terms of C_L and C_D were interestingly not observed in the range of 0.4×10^6 to 1.0×10^6. Matsumoto, *et al*. (2008) observed the vortex-induced excitation and Karman vortex excitation around the 2D rectangular cylinder with the aspect ratio of 4 and investigated the role of vortex-generation on the torsional flutter instability by changing the rotation axis, which is interesting to find the vortex-induced excitation as triggering of torsional flutter instability.

The most obvious example is for bodies at an angle to the approach flow, on which strong conical vortices appear, similar to those above delta wings. Such vortices are often less affected by changes in upstream flow characteristics, partly no doubt because they are usually a much more persistent feature of the generally unsteady flow; see e.g. Kawai (2002) for a discussion of their dynamics. There were some numerical predictions around 2D & 3D rectangular prisms (see e.g. Yu and Kareem 1998, Taylor and Vezza 1999). However, most of them had specific sizes and were not placed under our category.

In a recent experimental study of turbulent flow past a cubic obstacle(i.e. Lim, *et al*. 2007, hereafter denoted by LCH), it was found that while the details of the mean flow on the top of the cube, for example the mean pressure coefficients and the reattachment length, were approximately independent of the Reynolds number, as might be expected for sufficiently large values, the fluctuating pressure coefficients in contrast were not interestingly independent of the Reynolds number. In addition, there remain doubts about the mean-flow Reynolds number independence for other generic sharp-edged body shapes (rectangular objects of a wide variety of heights and aspect ratios) particularly those which produce flows containing strong, relatively steady concentrated vortices, or not, depending on their orientation.

The immediate emphasis in this paper is on the rectangular body with various aspect ratios. The aspect ratio is responsible for the type of generated wake and, ultimately, for the structural loading and pressure and especially structure excitation. For example, the drag coefficient of an elongated

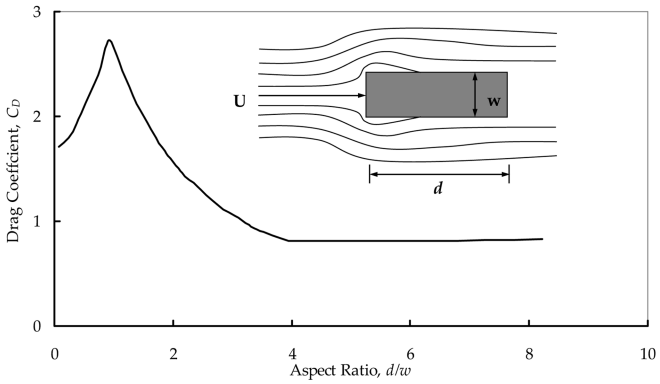

Fig. 1 Drag coefficient versus aspect ratio of rectangular body (Simiu and Scanlan 1996)

rectangular-section body in a flow is a function of the width of the body.(see Fig. 1) As shown in the figure, the drag is a function mainly of the elongation *d/w* of the body. Therefore, the paper consists of a carefully designed set of experiments on boundary layer flow over a surface-mounted rectangular obstacle, undertaken in an atmospheric boundary layer wind tunnel, of various speeds to allow variation in *Re* by a factor of 3-4 to be achieved with little change in upstream-boundary-layer characteristics. Data is also presented with the previous field and wind tunnel measurements, yielding a further order-of-magnitude change in *Re* and confirming the present wind tunnel experiments.

The wind-tunnel flows were designed to be similar to the (rural) atmospheric boundary layer. Here, main emphasis is placed largely on the extent to which the flows were affected by *Re* and attention is concentrated on the three cases defined by body's aspect ratios of 1 to 4 (in detail $40^d \times 80^w \times 80^h$, $80^d \times 80^w \times 80^h$ and $160^d \times 80^w \times 80^h$ in mm). The latter case typifies flows in which the wide or long vortex regions exist over the obstacle; the former is, in that respect, very different. The following section outlines the experimental techniques, Section 3 summarizes the flow characteristics in wind-tunnel boundary layers approaching the rectangular obstacles and also presents and discusses the major results; Section 4 gives the major conclusions.

2. Experimental techniques

2.1. Atmospheric boundary layer wind tunnel

Fig. 2 illustrates the set-up, showing the model location in the wind tunnel. Experiments were conducted in the middle closed-circuit subsonic wind tunnel, whose working section dimension is 0.6 m × 0.72 m × 6 m long having a maximum wind speed of about 40 m/s, within the Department of Mechanical Engineering at the Pohang University of Science and Technology(abbrv. POSTECH) in South Korea. It is suitable for generating an artificial boundary layer and is also equipped with modern hot-wire anemometry (IFA100) and a PIV system(Results from PIV system will be discussed in future publications) for optical measurements of the airflow.

2.2. Simulated atmospheric boundary layer

Thick boundary layers were generated using a technique often employed by wind-engineering

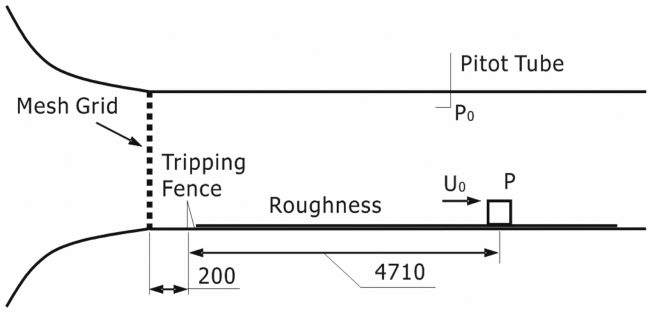

Fig. 2 The 0.6 m × 0.72 m wind tunnel test section and model setup

practitioners, first devised by Cook (1978). Toothed barriers spanning the floor of the working section near its entry, followed by a square section, bi-planar mesh across the entire working section and an appropriate rough surface thereafter can together be designed to yield mean-velocity profiles which are closely logarithmic over a significant portion of the working-section height, with turbulence stresses and spectra similar to those found in atmospheric neutrally stable boundary layers.(see Fig. 2) There are other ways of simulating atmospheric boundary layers (see Hunt and Fernholz 1975, for an old, but still appropriate, review); this particular method has the advantage of maximizing the depth of the logarithmic region but the disadvantage of not simulating the largest-scale eddies in the upper part of the atmospheric boundary layer. For the present purposes, since it was intended to make comparisons with the existing data such as wind tunnel and field data(e.g. a 6m height cube in Silsoe, UK) - less than one-tenth of the height of the logarithmic region - maximizing the depth of this region was deemed most important. It is crucial to design the barrier wall and mixing grid geometries in tandem with the intended roughness, since any mismatch will yield unacceptably long fetches before reasonably well-developed flows are attained. In the present case, commercially available artificial plastic artificial grass was used to provide the surface roughness. This gave a roughness length, z_0, of 0.17 mm, where z_0 is defined in the usual way via the mean velocity log law expressed as:

$$\frac{U}{u_*} = \frac{1}{\kappa}\ln\frac{(z-d)}{z_0} \tag{1}$$

where u_* and d are the friction velocity ($\sqrt{\tau_{wall}/\rho}$) and 'zero plane displacement', respectively. Obtaining the three unknowns (u_*, d and z_0) from the mean velocity profile alone is, as is well-known, a very ill-conditioned process. In the present study, u_* was deduced from an extrapolation of the measured turbulence shear stress ($-\overline{uw}$) to the surface (see Lim, *et al*. 2007), with d and z_0 then following from a best fit of the mean velocity data to Eq.(1). In the tunnel, the barrier wall had a height of 50 mm, with triangular cut-outs at the top, of pitch 50 mm and depth 50 mm, and the mixing grid consisted of a biplanar grid of 10 mm bars at a pitch of 50 mm.

2.3. Rectangle-body models and measurement systems

Smooth-surface rectangular bodies of height h equal to 80 mm were used in the tunnel and were fitted with 0.8 mm i.d. pressure taps at numerous salient points on the top surface and the front and

side faces.(see Fig. 3) Table 1 shows the rectangular models used in the study which is made of plexiglass, and it consists of 3 bodies - a cube ($80^d \times 80^w \times 80^h$ in mm) for comparing the existing results in a reference, two rectangular bodies ($40^d \times 80^w \times 80^h$ and $160^d \times 80^w \times 80^h$), and especially the flow around rectangular bodies could make two more aspect-ratios rotating it 90°. Standard tube connections to a (Furness FC-012) micromanometer allowed the measurement of mean surface pressures. Mean-velocity and turbulence-stress data within the boundary layers at the (subsequent) model locations and around the bodies themselves were obtained using a hot-wire anemometry (HWA). For HWA measurement, errors caused by inadequate yaw response were minimizd by using crossed-wire probes with the standard ±45° wires (Dantec 55P61, Miniature cross-wire) and employing the effective-cosine-law method to calibrate for yaw sensitivities. The probes had about 5 μm diameter and 1.25 *mm* long platinum-plated tungsten wires and were driven by IFA100 (TSI) CTA bridges, with outputs filtered to avoid aliasing and massaged by appropriate gain and offset to allow the best use of the analogue-digital converters (NI PCI-MIO-16E-1). Calibrations were performed against a standard pitot-static tube using the same micromanometer as was used for the (static) pressure measurements, and all analogue signals were digitized and passed to a desk-top computer. The pressure difference between the surface pressure p around the surface of the body and the reference pressure p_r was normalized by the dynamic pressure with free-stream velocity U_r and air density ρ to give the surface pressure coefficient C_p, which is denoted by $C_p = (p - p_r)/(0.5\rho U_r^2)$. Specialized software ('Virtual instruments', written in National Instruments' LabVIEW) allowed on-line calibration and measurement of all necessary quantities. The probes

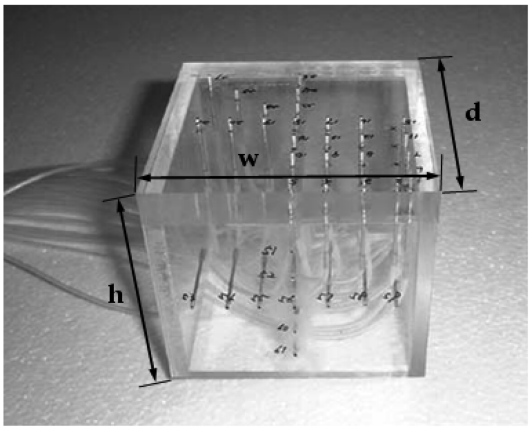

Fig. 3 A cube model ($80^d \times 80^w \times 80^h$ in mm) and pressure tappings

Table 1 Models used in the wind tunnel study (unit: mm)

No	ω	d	h	$\omega \times d$	w × d × h	ω/d	Abbrev.
1	80	80	80	6,400	512,000	1	1 × 1
2	160	80	80	12,800	1,024,000	2	2 × 1
3	80	160	80	12,800	1,024,000	0.5	1 × 2
4	80	40	80	3,200	256,000	2	2 × 1s
5	40	80	80	3,200	256,000	0.5	1 × 2s

were supported on traverse systems driven by the same computer. Sampling rates were typically between 2kHz and 10kHz, depending on the quantities being measured, with sampling times of 60-120s.

3. results and discussion

3.1. Generation of the deep turbulent boundary layer

All mean- and fluctuating-velocity data were normalized using the mean velocity at the cube height, U_h. The mean-velocity profiles obtained over a range of wind speeds in the tunnel are shown in Fig. 4. Special care was devoted in selecting turbulent boundary layer generation procedures as close as possible to natural atmospheric mechanisms, according to modern boundary layer wind tunnel technique. The measurements were made at different longitudinal locations of x/h = 6.4, 21.5, 34.8 and 58.9, which was with the aim to check that the simulated flow would finally be a fully developed shear flow specifically designed to be similar to the (rural) atmospheric boundary layer. The combination of the square section, bi-planar mesh and toothed barriers at the entrance of the test section generated the initial wake impulse on the tip of the barriers to make a big peak and induce the high turbulence intensity at a certain height (≈ 1.0) surrounded by background turbulence and it was gradually decreased in the far downstream.(see Fig. 4) Consequently, the mean velocity profile had also shown an abrupt change of velocity magnitude in early stage and all overlapped in which the model will be placed. The main goal was to achieve the stable oncoming flows with the designed mean velocity used for comparing the existing results(i.e. LCH 2007) but with the similar turbulence structures of several different Reynolds numbers. In addition, for acquiring an adequate distribution of shear flows, the artificial grass was also selected in terms of adequate floor distribution of roughness elements. Fig. 5 shows the corresponding profiles for the Reynolds stress $-\overline{uw}$. The data do not extend to $z/h = 5$ in the tunnel but are quite adequate for demonstrating the fully developed profiles. It has been known that the stress profiles from the real field are almost constant close to the surface and gradually decreased with height,

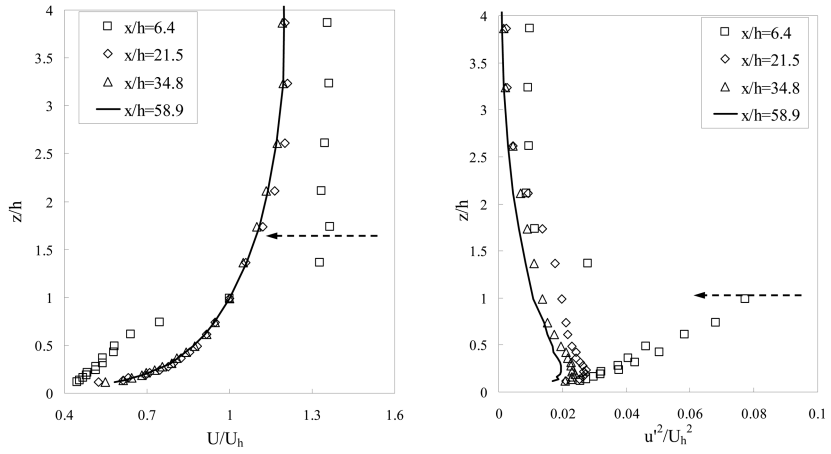

Fig. 4 Mean velocity (left) and turbulent intensity (right) profiles over different longitudinal locations in the tunnel, where the origin of x is at the location of the barrier wall

which is due to the less viscous effect (Lim 2007). Note that the intensities and stresses seem to be decreased with increasing distance downstream. This is almost certainly a result of generating artificial shear layer. The flow is probably still developing at this axial location ($x/h = 58.9$); this would account also for the slightly unstable shape of the stress profiles compared with those from the existing result (LCH 2007).

The (HWA) mean-velocity profiles obtained from a range of wind speeds in the tunnel are shown in Fig. 6. The profiles were obtained at the eventual model location, 4.7 m downstream from the tooth barrier wall in the tunnel. Notice in particular that the velocity ranges (ms^{-1} in unit) imply Re

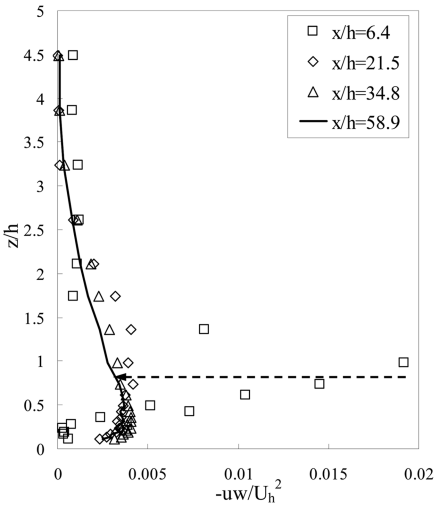

Fig. 5 Development of Reynolds-shear-stress profiles in the tunnel

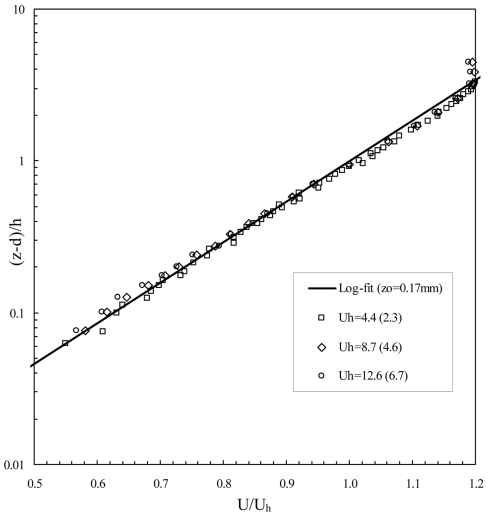

Fig. 6 Log-fitted mean velocity profiles at x/h ≈ 60 from the barrier wall. Figures for the velocity at model height, U_h, are in ms^{-1} with $Re \times 10^{-4}$ (based on the appropriate h in parentheses. The solid line gives the log law

number ($\mathrm{Re} = U_h h/\nu$) variations of $2.3 \times 10^4 \le Re \le 6.7 \times 10^4$ in the tunnel, and that in no place is there any significant profile change with *Re*. The three *Re* ranges overlap and yield a factor 3 variation in *Re*. The fits to solid line of log-law extend at least to $z = 2h$, so the models are submerged well within the log-law region. The roughness length, z_0 of 0.17 mm, stands for the flat open terrain and/or flat snow field from the Davenport roughness classification(Wieringa 1992). Here, emphasis is placed on the comparison with the existing results and attention is concentrated on the representative non-dimensional numbers, and Jenson number(*J*, which is defined as $J = h/z_0$), was one of them. In this study, *J* based on the roughness length and the body height, was around 470 and it was the appropriate order of magnitude. For instance, the *J* in the existing papers were 890, 750 in the wind tunnel and the real field (Richard and Hoxey 2004), respectively.

Fig. 7 presents longitudinal-velocity spectra, $E_u(f)$, obtained at $z = h$. All of the results are compared and shown in detail, in comparison with standard spectra for the atmospheric surface layer. In the figure, the spectra are plotted in the form in which collapse the inertial subrange of a logarithmic shape of -5/3 spanning from 0.1 to 1, which shows the energy transfer from at low frequency to high. Common reference data for the spectral shape is those standard formulas provided by ESDU(Engineering Sciences Data Unit 1985) and by the wind tunnel data of LCH(2007). The ESDU spectral shape used in this study is described as follows:

$$\frac{fE_u(f)}{\overline{u'^2}} = \frac{4n'}{(1 + 70.8n'^2)^{5/6}} \tag{2}$$

where $n' = fL_x/h$ and L_x is the longitudinal integral scale. This is equivalent to the Kaimal spectrum (1978) in the inertial subrange if L_x is related to the turbulence statistics via $L_x/h = 0.237(\overline{u'^2}/u_*^2)$. The resulting spectra provided satisfactorily consistent data within a factor of three in Re. Note that the data in the inertial subrange appear to collapse quite well. However, this kind of plot can be misleading in this respect since the spectral density is normalized by a turbulence parameter (u_*^2 in this case). (See LCH(2007) for further discussion).

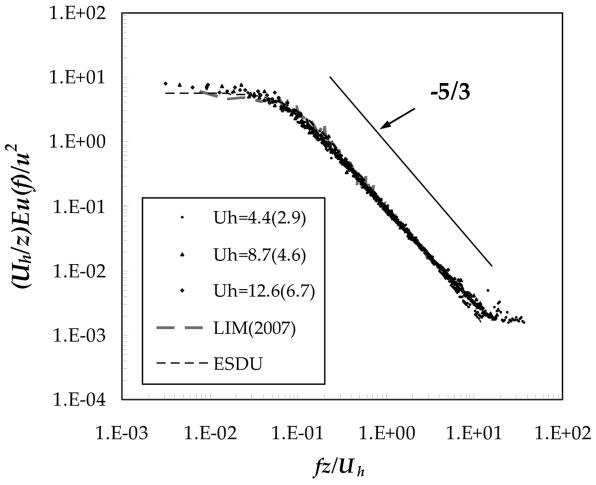

Fig. 7 Spectra of the axial turbulence component at $z = h$ normalized by u with $\mathrm{Re} \times 10^{-4}$ values given in brackets

3.2. Surface pressure distribution - a cubical model (1×1)

I consider first the surface pressure field around the 1 × 1 model. Fig. 8 presents the variation of the mean static pressure C_p along the axial centreline of the cube obtained in the wind tunnel and compares the existing results, as a function of the measurement location *x/h*; $x = 0$ corresponds to the foot at the front face of the model body - actually depending on the wind direction, see the solid line on the right figure. The wind tunnel data provides around a factor of 3 in *Re* (the typical *Re* was 4.6×10^4, the reference wind tunnel and field data spans up to around 280×10^4). C_p is defined as $(p\text{-}p_r)/\{(0.5\rho U_h\text{^}2)\}$, where p_r is the mean static pressure in the upstream flow. For the wind-tunnel data, this was obtained in the free stream upstream of the models; the variation vertically through the flow was negligible. The profiles in the figure have the expected shape, in that the largest negative pressures occur just beyond separation at the leading edge and are followed by a substantial pressure recovery on the top surface, as shown frequently by previous studies. Note that the data agree well with the earlier field data of Richard and Hoxey (2004) but are significantly different from the wind-tunnel data of CR. The latter are similar to those of Murakami and Mochida (1988) and, in agreement with CR's discussion, are undoubtedly a result of very much higher upstream turbulence levels, leading to much earlier attachment and pressure recovery on the top surface.

The immediate implication of the data in the figure is that there appears to be little Reynolds-number effect. Not surprisingly, this was already pointed out the existing literature(See LCH(2007)). Note that the rest of the subsequent figures are arranged in a similar manner to this figure, i.e. transect profiles. The fact that even the small-scale data in the figure show no variation over a factor of over 60 in *Re* including the field measurement would immediately suggest little likelihood of change with further increases in *Re*. Note, however, that at the location near the leading edge there is a hint of a small *Re* effect at the lower end of the *Re* range. However, once *Re* exceeds about 3×10^4, the changes are very small; this is consistent with the existing literature (see LCH).

Figs. 9 and 10 show the mean surface static pressure along the mid-height and the transverse centreline of cube, respectively. Similar to the result at the Fig. 8, the surface pressure profiles are almost identical to each other, except the CR's result. This can also be explained that, as described above, the higher upstream turbulence levels in the approaching flow make the attachment and pressure recovering earlier. The profiles in the Fig. 10 also have the expected shape, in that the largest negative pressures occur just in the middle of top-surface of cube and are followed by a

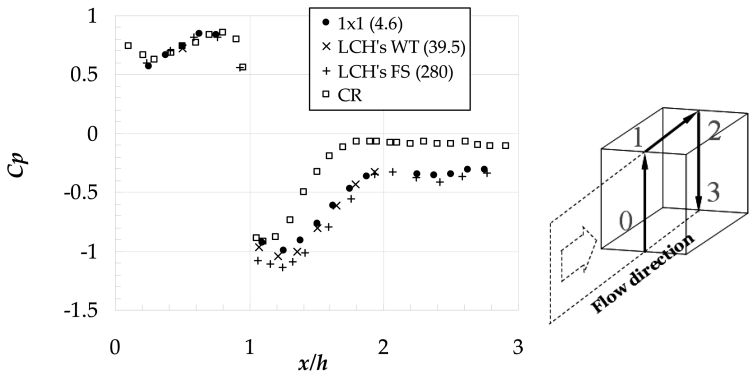

Fig. 8 Mean surface static pressure along the central section with wind normal to face

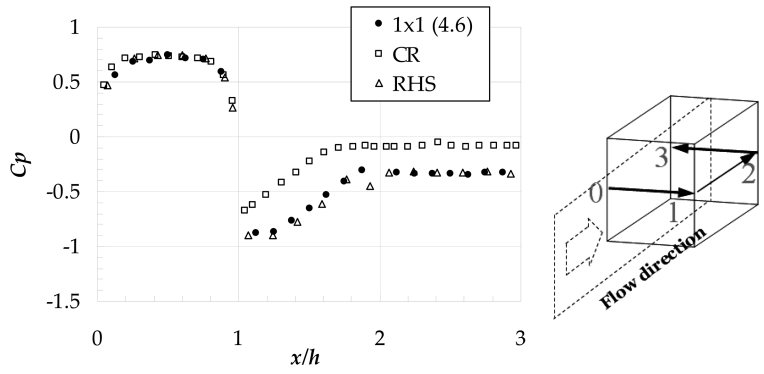

Fig. 9 Mean surface static pressure at the mid-height of cube. (Lim, *et al*. 2007, Hoxey, *et al*. 1998)

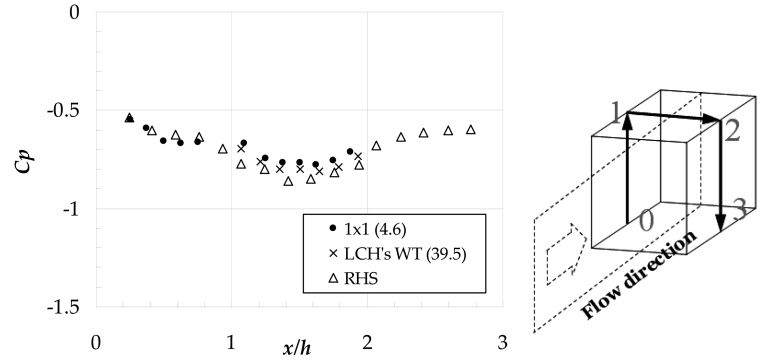

Fig. 10 Mean surface static pressure along the transverse centreline of cube

gradual pressure recovery associated with the separation and attachment range on the top surface and side surface, as shown frequently in previous studies (see CR). Note that the data from both figures are surprisingly similar to the field data (at $Re_h = 2.8 \times 10^6$) which were obtained in similar conditions (e.g. Jenson number, turbulent intensities, spectra) as those of the current wind-tunnel boundary layer, although of course at a very much higher Reynolds number.

Even though the current data in this section are showing the simple comparison with the existing results, the immediate implication is that the comparison with the existing results confirms the high accuracy and reliability of the current study, and the identical condition with the field measurement yields the significant reduction of the measurement errors. Therefore, the current section could be a precursor of the rest of the pressure profiles and the next section will discusses the pressure profiles around the rectangular obstacles with the same boundary layers.

3.3. Surface pressure distribution - models with aspect ratio

Mean surface static pressure profiles along the centerline of the models with the three different aspect ratios are plotted in Fig. 11. The figure shows how the surface pressure on the top as well as on the front and rear face changes with changing of the width of the body. Note that several subsequent figures are arranged in a similar manner to Fig. 11, i.e. the pressure profiles are shown

on the left and models to compare each other are shown on the right, to easily visualize the measurement locations around the body. The suction pressure on the top surface along the centerline is obvious from these profiles, that is, the wider the shape of the body, the stronger is the surface suction pressure on the top surface. It should also be noted that these surface pressure profiles reflect the flow features with different aspect ratio discernible in the surface profiles of the body. It is also noted that interestingly the front and rear face of the body has little surface pressure variations so that these results demonstrate the effect of the 3-dimensional flow passing the side of the body. (see Fig. 9) The immediate implication of the data in Fig. 11 is that the width variation while maintaining the depth makes the surface pressure on the top surface more negative, whereas the front and rear face are almost consistent for the width variation. In addition, as it can be seen, the solid arrow shows the direction of the pressure drop as the width changes.

In Fig. 12, the mean surface static pressure along the side face at the mid-height of the three different boxes with changing transverse width is presented. The abscissa in the figure is normalized with the body height. As consistent with the previous figure, the pressure drop with increasing width was noticeable to the negative direction. These results demonstrate that with an increase in

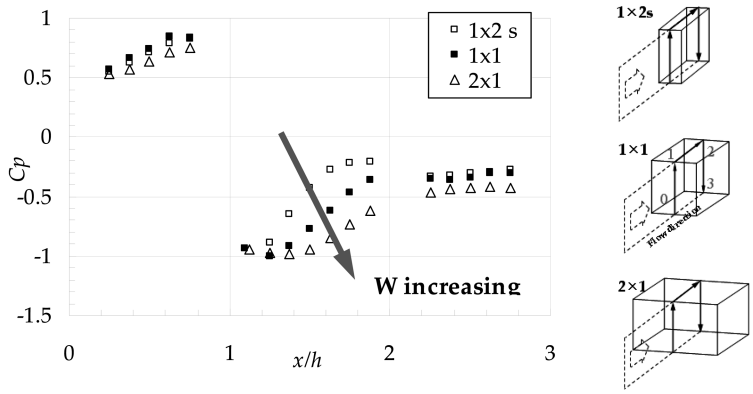

Fig. 11 Mean surface static pressure along the centerline of the three different boxes with changing transverse width

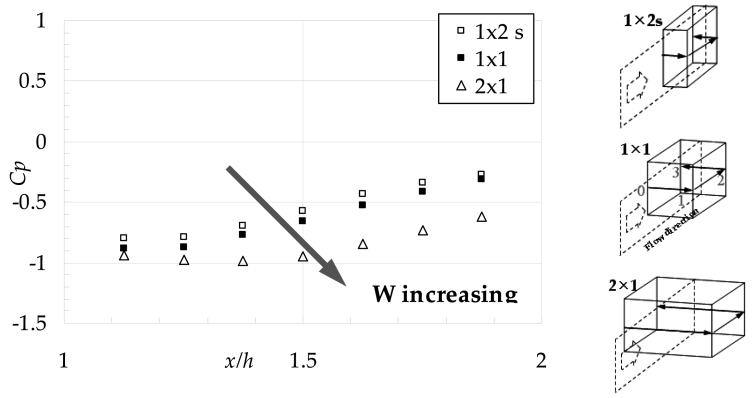

Fig. 12 Mean surface static pressure along the centerline of the three different boxes with changing transverse width

the horizontal width, i.e. as increasing the aspect ratio, there is a concurrent suction pressure drop on the side face. The pressure difference between 1 × 2s and 1 × 1 was not significant, but this seems to be a minor error causing from the measurement error. One might regard these pressure differences as the wind tunnel blockage effect from the area ratio of the model and the tunnel section, but the total area of the test section was 4,320 cm^2 and the frontal area of the widest cube (e.g. 2 × 1 model) so that the maximum blockage effect was at most 2.8%.

Figs. 13 and 14 show the mean surface static pressure profiles along the centerline of the models with changing longitudinal length(i.e. the depth) - 2 × 1s, 1 × 1 and 1 × 2. The different size of the depth maintaining the front face area makes different length of the side face - the ratio of 1:2:4, respectively. The flows around wall-mounted sharp-edged models usually have separation and often attachment around the body so that the pressure profiles in the figure have the similar shape, as shown in the above results. In the case of the narrow depth model (2 × 1s) of the Fig. 13, it is not clear, but it can be conjectured that a separation and a recirculation region behind the model might exist. The pressure profiles of the models 1 × 1 and 1 × 2 seem to have a similar trend and it is noted that the overall distribution of the surface pressure makes good agreement and the

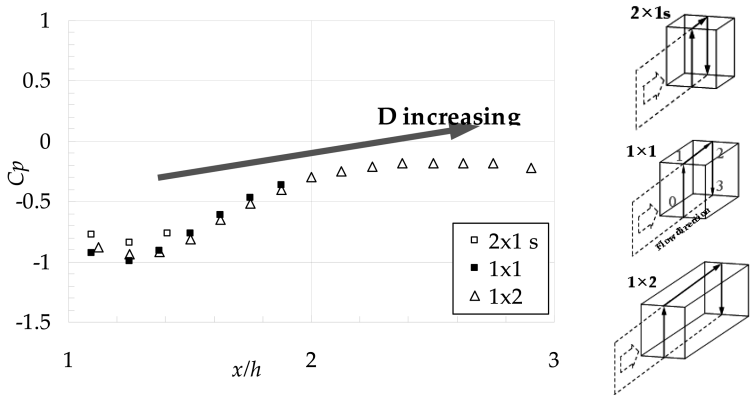

Fig. 13 Mean surface static pressure along the centerline of the three different boxes with changing longitudinal length

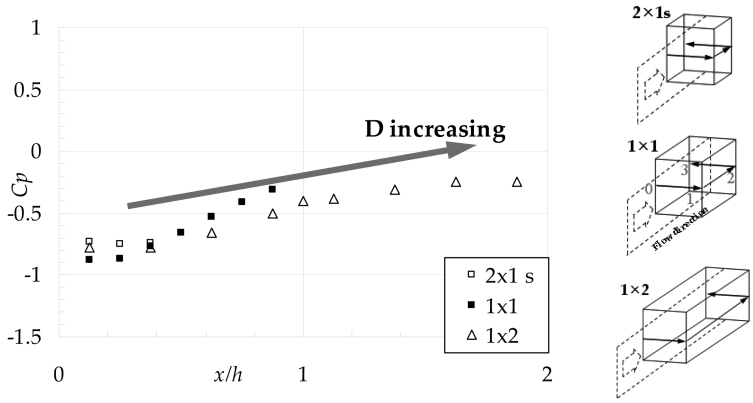

Fig. 14 Mean surface static pressure along the centerline of the three different boxes with changing longitudinal length

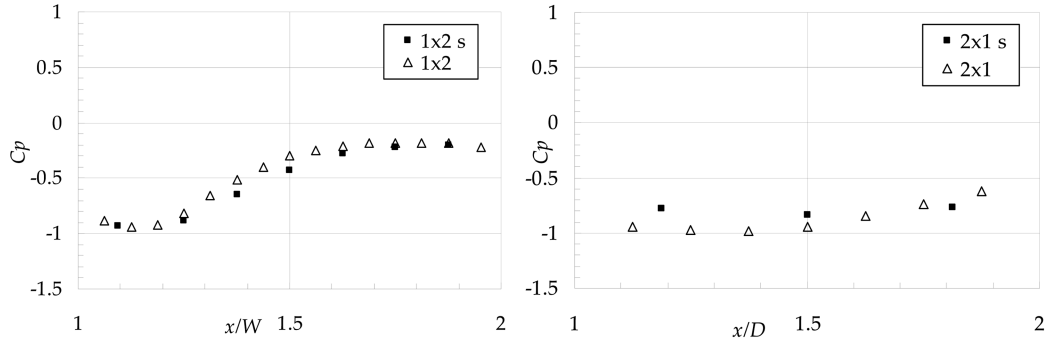

Fig. 15 Mean surface static pressure along the centreline on the various boxes with the normalization of width (W) and the depth (D), respectively

longitudinal length of the body only affects the recovery region on the top surface (see Fig. 14, but there appears a little discrepancy in the side face, which will be discussed in the next paragraph.

Fig. 15 presents the variation of the mean static pressure C_p appropriately normalized as described in section 3.2. Note that the abscissa in the previous section was presented as a non-dimensional axis normalised by a body height h, whereas the current axes are normalized along the the axial centerline of the models by the characteristic length - the width (W, width effect) and the depth (D, the depth effect), respectively. In the figure, they are generally in good agreement. Therefore, it can be described that even though the length and width of the rectangular body and the Re numbers are changed, the characteristics of the static surface pressure profiles along at least the centerline itself remains unchanged, even if any, it ought to be small scatter. It is difficult to avoid the general conclusion here that, provided the bluff-body geometry with aspect ratio is not such as to yield strong, relatively steady, vortical motions, Re effects on the mean pressure field are not significant; otherwise, however, and in certain regions of the flows with aspect ratio, there is some effect. C_p data collected at points near the top and the side axial edges do not show Re effects occurring within regions near separation lines; only if the separation leads to unusually strong and concentrated vortex motions do such effects occur.

4. Conclusion

This study has shown that it is possible, at a given model scale (with fixed body height), to vary the Reynolds number by at least a factor of three whilst maintaining identical non-dimensional characteristics of the upstream boundary layer. The newly performed wind tunnel measurement has been carried out to compare the shape effect of a bluff body, and then to find out the ventilation effects and wind characteristics. The velocity and pressure measurements were useful to rougly find the flow characteristics around the rectangular bodies, and these preliminary databases seem to be sufficient to capture the surface pressure characteristic around the bodies and in the near future. This study needs to do the further consideration on the shedding and evolution of the unsteady vortex shedding from the body. Although only experimental study have been presented in this paper, from previous experience of similar measurements it is expected that the current data provides good reference data for the future study.

Acknowledgement

The author wish to thank the wind-tunnel staffs for their help and Prof. Sang-Joon LEE in the Department of Mechanical Engineering, Pohang Univ. of Sci. and Tech. for his cheerful comments. Likewise, the help of Mr. Tae-Yoon JEONG (PuKyong Nat'l Univ.) and Ms. Su-Jin Lee (Pusan Nat'l Univ.) was crucial and is gratefully acknowledged. This work was supported by PuKyong National University Research Fund in 2006(PKS-2006-023).

References

Castro, I.P. and Robins, A.G. (1977), "The flow around a surface mounted cube in uniform and turbulent streams", *J. Fluid Mech*., **79**, 307-335.

Cherry, N.J., Hillier, R. and Latour, M.E.M.P. (1984), "Unsteady measurements in a separating and reattaching flow", *J. Fluid Mech.*, **144**, 13-46.

Cigada, A., Malavasi, S. and Vanali, M. (2006), "Effects of an Asymmetrical Confined Flow On a Rectangular Cylinder", *J. Fluids Struct*., **22**, 213-227.

Cook, N.J. (1978), "Wind tunnel simulation of the adiabatic atmospheric boundary layer by roughness, barrier and mixing device methods", *J. Wind Eng. Ind. Aerod*., **3**, 157-176.

Davenport, A. (1999), *The missing links - Plenary paper in Wind Engineering into the 21st Century*, ed. A. Larson & F. M. Livesey.

Djilali, N. and Gartshore, I.S. (1991), "Turbulent flow around a bluff rectangular plate. Part 1: experimental investigation", *J. Fluids Eng*., **113**, 51-59.

ESDU (1985), *Characteristics of atmospheric turbulence near the ground. Part II: single point data for strong winds (neutral atmosphere)*, Engineering Sciences Data Unit, Item 85020.

Hoxey, R.P., Reynolds, A.M., Richards, G.M., Robertson, A.P. and Short, J.L. (1998), "Observations of Reynolds number sensitivity in the separated flow region on a bluff body", *J. Wind Eng. Ind. Aerod.*, **73**, 231-249.

Hunt, J.C.R. and Fernholz, H.H. (1975), "Wind-tunnel simulation of the atmospheric boundary layer: a report on Euromech 50", *J. Fluid Mech.*, **70**, 543-559.

Kaimal, J.C., Wyngaard, Y., Izumi, O.R. and Cote, O.R. (1978), "Spectral characteristics of surface layer turbulence", *Q. J. Roy. Meteor. Soc*., **98**, 563-598.

Kawai, H. (2002), "Local peak pressure and conical vortex on a building", *J. Wind Eng. Ind. Aerod.*, **90**, 251-263.

Larose, G.L. and D'Auteuil, A. (2008), "Experiments on 2D Rectangular Prisms at High Reynolds Numbers in a Pressurised Wind Tunnel", *J. Wind Eng. Ind. Aerod*., **96**, 923-933.

Lim, H.C. (2007), "Generation of a turbulent boundary layer using LES", Trans of the KSME (B), **31**, 680-687.

Lim, H.C., Castro, I.P. and Hoxey, R.P. (2007), "Bluff bodies in deep turbulent boundary layers Reynoldsnumber issues", *J. Fluid Mech.*, **571**, 97-118.

Matsumoto, M., Yagi, T., Tamaki, H. and Tsubota, T. (2008), "Vortex-induced Vibration and Its Effect on Torsional Flutter Instability in the Case of B/D=4 Rectangular Cylinder", *J. Wind Eng. Ind. Aerod*., **96**, 971-983.

Richards, G.M. and Hoxey, R.P. (2004), "Quasi-steady theory and point pressures on a cubic building", *J. Wind Eng. Ind. Aerod*., **92**, 1173-1190.

Simiu, E. and Scanlan, R.H. (1996), *Wind Effects on Structures*, Wiley, New York.

Taylor, I. and Vezza, M. (1999), "Prediction of unsteady flow around square and rectangular section cylinders using a descrete vortex method", *J. Wind Eng. Ind. Aerod*., **82**, 247-269.

Tieleman, H.W. and Akins, R.E. (1996), "The effect of incident turbulence on the surface pressures of surfacemounted prisms", *J. Fluids Struct*., **10**, 367-393.

Wieringa, J. (1992), "Updating the Davenport Roughness Classification", *J. Wind Eng. Ind. Aerod*., **41-44**, 357-368.

Yu, D. and Kareem, A. (1998), "Parametric study of flow around rectangular prisms using LES", *J. Wind Eng. Ind. Aerod*., **77&78**, 653-662.

CC